Virtual prototyping: A case study of positioning systems for drilling operations in the Barents Sea

Pierre Major*, Robert Skulstad, Guoyuan Li, Houxiang Zhang

Department of Ocean Operations and Civil Engineering, Norwegian University of Science and Technology, Ålesund, Norway

*Corresponding author: Pierre Major, e-mail: pierre.major@ntnu.no

Pierre Major received his M.Sc degree in Information Technology and Electrotechnique from the Swiss Federal Institute of Technology of Zürich (ETHZ) in 2005. After various positions in the software industry, became head of research at Offshore Simulator Centre in 2019. He is currently working as an industrial Ph.D. candidate at the Norwegian University of Science and Technology (NTNU), Ålesund. His domains of interests are virtual prototyping, real time simulation and machine learning.

Robert Skulstad received his M.Sc. degree in Engineering Cybernetics from the Norwegian University of Science and Technology (NTNU), Trondheim, Norway, in 2014. He is currently working at NTNU, Aalesund, Norway, as part of the Mechatronics Laboratory within the Department of Ocean Operations and Civil Engineering, as a Ph.D. candidate. His research interests include ship motion prediction, machine learning and ship motion control.

Guoyuan Li received a Ph.D. degree from the Institute of Technical Aspects of Multimodal Systems (TAMS), Department of Informatics, University of Hamburg, Hamburg, Germany, in 2013. In 2014, he joined the Mechatronics Laboratory,

Department of Ocean Operations and Civil Engineering, Norwegian University of Science and Technology, Norway. In 2018, Dr. Li became an associate professor in ship intelligence. He has extensive research interests including eye tracking analysis, modeling and simulation of ship motion, artificial intelligence, optimization algorithms and locomotion control of bio-inspired robots. In these areas, he has published over 40 journal and conference papers.

Professor Houxiang Zhang, D.Sc., received his Ph.D. degree in mechanical and electronic engineering from Beijing University of Aeronautics and Astronautics, China, in 2003. From 2004 to 2011, he worked as a postdoctoral fellow at the Institute of Technical Aspects of Multimodal Systems, Department of Informatics, Faculty of Mathematics, Informatics and Natural Sciences, University of Hamburg, Germany. Dr. Zhang joined the Department of Ocean Operations and Civil Engineering, Norwegian University of Science and Technology in Aalesund, Norway, since April 2011, where he is a full professor on robotics and cybernetics. Currently, he also has a gift professorship on product and system design from the industry. Dr. Zhang's research focuses on maritime operation and mobile robotics. In these areas, he has published over 150 journal and conference papers and book chapters as author or co-author. He received the best paper award at the IEEE/AEME AIM2008 conference, and three finalist awards for best conference paper at IEEE Robotics and Automation conferences.

Virtual prototyping: A case study of positioning systems for drilling operations in the Barents Sea

This study proposes a framework for comparative study on three different positioning solutions for mobile offshore drilling units (MODUs) using high modulus polyethylene (HMPE) ropes, including active mooring with an HMPE rope, conventional dynamic positioning (DP) and active hybrid position-keeping (AHP-K). The goal of the positioning systems is to keep the MODU above the wellhead with acceptable riser-angle loading, minimal energy consumption, reduced underwater noise generation, and harmful emissions. This is the first time a holistic study has been performed on positioning that factors in the financial and environmental costs. The time domain simulation, which includes sea-state, wind, and current profiles, is performed with a well-developed software architecture and control algorithms for MODU position-keeping. The case study addresses a MODU drilling in the Barents Sea. Simulation results show that AHP-K is more efficient compared to the other two positioning solutions for drilling operations in the studied environment.

Keywords: Barents Sea, Environmental Cost Estimation, Framework for Simulation Integration, Hybrid Mooring Position Keeping, Time domain Simulation, Virtual Prototyping

1 Nomenclature

A	Cross section area [m^2]
A_i	Amplitude of ith wave component [m]
C	Cost of one metric ton of marine diesel oil (MDO) [$/T]
$E_T(t)$	Average energy consumed by the thruster during the sampling time step Δt at time step t [kJ]
$\boldsymbol{e}_p$	Position error vector
E_E	Energy consumed by the engine during the sampling time step [kJ]
E_{Oil}	Energy density of MDO [MJ/kg]
F_{CO_2}	Tons of CO_2 per consumed ton of MDO [T/T]
F	Tension force along the rope [N]
F_{NO_x}	Tons of NO_x per consumed ton of MDO [kg/T]
$\mathrm{h}(\vec{\mathrm{x}},\mathrm{t})$	Wave elevation at point $\vec{\mathrm{x}}$ [m]
$\vec{k}_i$	Wave number of the i^{th} wave component $\vec{k}_i = (k_i \cos\theta_i\,, k_i \sin\theta_i)$; [1/m]
k_1	Scaling factor
L	Rope length
M_{Oil}	Tons of consumed MDO
M_{CO_2}	Tons of CO_2 emitted
M_{NO_x}	Kilograms of NO_x emitted
$\boldsymbol{p}_B$	Current rig position
$\boldsymbol{p}_A$	Set rig position
T(t)	Thrust developed by the thruster [kN]
T_{cost}	Total cost in [$]
$\boldsymbol{u}_{tot}$	Total speed command of a winch
u_{winch_i}	Commanded speed of winch i [m/s]
ΔL	Rope longitudinal elongation [m]
Δt	Sampling time step [s]
η	Mechanical and thermodynamic efficiency (Engine, Transmission)
$\alpha(t)$	Cross-fading factor during transition, $\alpha(start) = 1,\ \alpha(end) = 0$
σ	Youngs's modulus [GPa]
θ_i	Direction of the i^{th} wave component, a spreading function is used to distribute the waves around the main direction, with θ_i= 0 being north. Clockwise rotation.
φ_i	Phase of i^{th} wave component (a random number) [1]
ω_i	Temporal frequency of the i^{th} wave component [1/s]
$\angle\boldsymbol{e}_p$	Bearing of the desired rig position [degrees]
$\angle winch_i$	Angle between the forward axis of the rig and winch i [degrees]

1 Introduction

The Norwegian Petroleum Directorate expects the number of survey drillings in the Barents Sea to increase (NPD 2017). The Barents Sea is a key area for sea mammals and fish species like cod, which is a major economic resource for Norway and Russia. Dynamic Positioning (DP) systems are major enablers of offshore oil exploration, yet they consume a lot of energy and emit noxious gases and noise. Underwater anthropogenic noise and its consequences for aquatic life is a growing concern to the scientific community (Williams et al. 2015). Moreover, since the sharp fall of oil price in 2014, oil operators have introduced major cost cutting programs. Saving fuel has both financial and environmental impacts. In Norway, the NOx Fund subsidises NOx abatement projects, making low emission profiles of the otherwise taxable gas financially attractive.

DP systems are thus ripe for innovation. The purpose of a DP system is to keep floating drilling units within a specific watch circle, which is a criterion combining the maximum position and heading errors. A mobile offshore drilling unit (MODU) must be kept above the wellhead with minimal energy consumption, and maximal positioning accuracy to minimise the stress between the drill string blowout prevention system (BOP) and the well underneath. If the drilling unit drifts off while connected to the wellhead, massive leakages of drilling muds, gas, or oil may occur. While line chain mooring and load reducing thruster assistance (TA) position mooring systems have in use for decades, (Aamo and Fossen 2009), the heavy chains they require to moor the floating units tend to damage the seabed. They can also be complex and dangerous to

handle, leading to casualties such as the Bourbon Dolphin accident in 2007. High modulus polyethylene (HMPE) ropes provide an excellent alternative to wires and chains. Being neutrally buoyant, immersed fibre ropes neither add extra payload on the winches or towing vessel, nor lie on the seabed as chains normally do, thereby preserving corals and other sea life habitat. Being extremely tension resistant with minimal stretch, they have been used for many years in permanent moorings in waters more than 1500 m deep (Leite S. and Boesten J. 2011). In such water depths, the weights of the chains are too challenging to handle. Therefore, this virtual prototyping (VP) study investigates a positioning method in which HMPE rope-based winches actively position the rig and are assisted by DP when necessary.

Researchers of mechanical engineering and product development consider Zorriassatine et al.'s (2003) categorization of VP methods valid for product design and manufacturing:

- visualization
- fit and interference of mechanical assemblies
- testing and verification of functions
- performance, evaluation of manufacturing and assembly operation
- human factor analysis.

This study suggests the addition of control systems design, test, and analysis because VP affects the engineers' approach to the products or procedures.

The aim of this paper is to examine the benefits of VP by testing a control algorithm on a truly innovative system that has not been produced before. The main contributions are:

1. The building of the realistic time domain model with performance faster than real time, only based on three-dimensional (3D) model.
2. The aggregation of rich environmental factors of a specific location in the Barents Sea and the dynamical environment simulation.
3. The creation and validation of an original positioning system which could potentially have both financial and environmental benefits.

The paper is organized as follows. Section 2 introduces current relevant work on time domain simulation. The system architecture and simulation model are described in Section 3. Section 4 presents the simulation results and Section 5 concludes the paper and opens future research directions.

2 Related Works

Recent research on VP include (Chu et al. 2017), which applies a VP framework to the mechanical, hydraulic, and control system design of a crane and advanced visualization in regular sea conditions using a sinusoid wave to represent the movement of the vessel. (Ham et al. 2017) investigate the movement of a drillship in regular seas; (Kim et al. 2014) show the design process of a winch/mooring-based control system with platform disturbances in the unconventional range of 1-15 Hz. (Ji et al. 2015) propose a position mooring system design for a barge using ropes/wires in which the motion controller and control allocation systems are unified. (Li et al. 2016) investigates ship model,

simulation, and control design using VP via an XML- and TCP-based simulation bus, which requires a tedious, error prone process to configure, and is slow to run. (Zhang et al. 2017) describes a mathematical model for virtual reality (VR) of a subsea installation which runs in near real-time, but the wave model only consists of one wave component and they ignored the role of the wind. The results are compared in one dimension with simulation benchmark from (OrcaFlex 2018), which is well-established software for time domain simulation of mooring of floating structures and offshore operations supporting rich environmental models, but only one environment state per simulation run. This means that one cannot build a scenario with dynamical sea state changes, which prevents immersive simulation or training control algorithms adapting to weather changes. (Yu et al. 2017) presents a full mission simulator relying on a similar VR system based on the physics engine Vortex and the visualisation Vega Prime, with validation of the simulation results with a benchmark from SESAM, a software suite for hydrodynamic and structural analysis of ship and offshore structures (DNVGL 2018), for various wave heights, not specifying the spectrum, but with wind and current. (Sha et al. 2018) investigates the effect of rich wave and wind spectra on the structure of a bridge over a deep fjord in the time domain. They use the time domain to account for non-linear responses that are non-trivial to solve in the frequency domain but calculate the frequency domain transfer functions in WADAM, a software for frequency domain analysis of stationary vessels (DNVGL 2018). The study focusses on structural response and not on real-time performance of the simulation. (Reite et al. 2014) describe FhSim, an object-oriented real-time time domain ship and aquaculture

simulator. It includes cables and nets, a rich environmental model, and a seakeeping response of the floating structure based on the low speed strip theory introduced in (Salvesen 1970) program ShipX Veres (ShipX 2018). But it does not support panel theory import such as WADAM or WAMIT (2018). This means that FhSim is appropriate for simulating slender structures, but not for offshore floating rigs.

None of the abovementioned studies combine heterogeneous system (rig, thruster, mooring winches, and fiber ropes) with rich environmental factors (JONSWAP spectrum, wind, and current) in a time domain simulation.

3 Method

3.1 Simulation description

The Island Innovator (Island Drilling 2018) depicted in Figure 1, has been used as a MODU model with high resolution 3D model consisting of tri-meshes for high fidelity aero- and hydrodynamics (drag coefficients) computation in the physics engine. Wind, current, and waves affect the MODU. The tensioners compensating the platform heave for the drill string connecting the MODU to wellhead via the BOP are modelled as a winch holding a constant tension. Four mooring winches, controllable by a positioning algorithm developed for the purpose of the study, are each connected to a suction anchor (N355m, E355m) (N355m, E-355m) (N-355m, E355m) (N-355m, E-355m) by a 76mm nominal diameter, 12 x 3 strand HMPE rope, made from the Dyneema® fibre type DM20 XBO. For the sake of simplicity, due to time and resource shortage, a single azimuth thruster is mounted at the barycentric position of the real thrusters.

The simulation design had to make a trade-off: the simulation must last long enough to provide significant results for each weather case and short enough to provide results quickly. The transition time must be chosen such that the weather transitions are not too sharp for the control algorithm, while keeping the total simulated time as low as possible. Each run lasts around 32000 seconds simulated time, of which only 7200 seconds are dedicated to measurements of the 300-second-long transitions between each weather case.

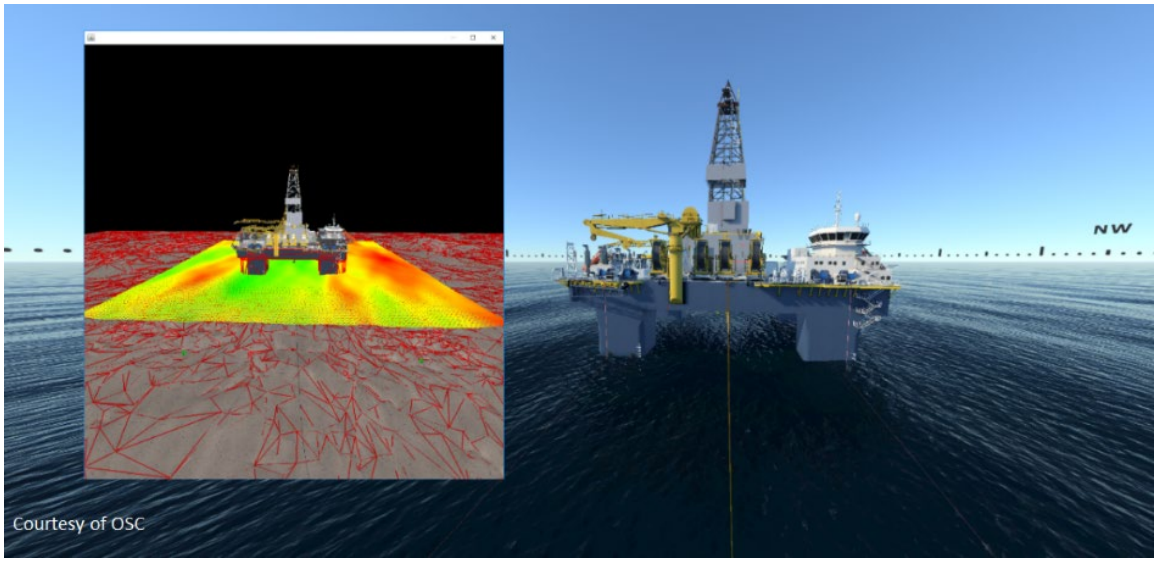

Figure 1. Visualization of wave pattern and sea bead (left), simulator view with highlighted rope tensions (right).

3.2 Software architecture and scene

Because of its support of multibody physics, its plug-ins philosophy, and its flexible integration to external systems, the Java-based simulation platform developed by OSC has been extensively used for equipment training, crew operation, procedure training, and VP of equipment, procedures, and operations. The simulator runs a time domain simulation which allows the physics engines to account for non-linear effects.

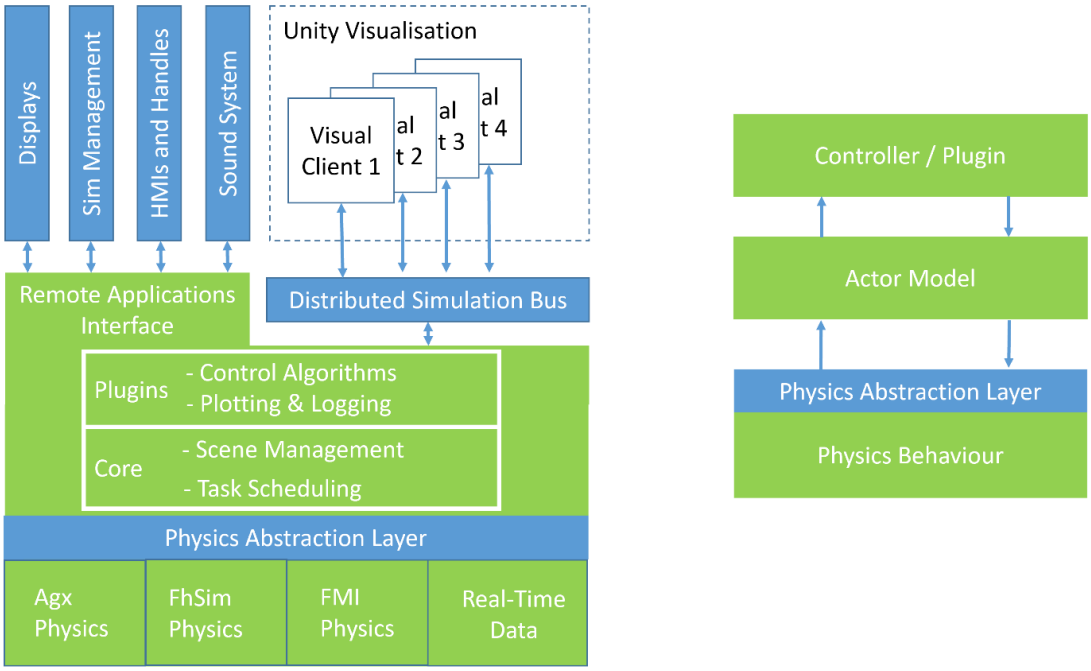

Figure 2. Software architecture (left) and schematic representation of actor model (right).

The behaviour of the simulated objects is implemented by physics engines underneath the abstraction layer (Figure 2), allowing flexibility in the choice of physics engine and a compromise between real-time constraints and model accuracy. In this case, the C++ based Agx physics engine (Algoryx 2018), with its arbitrary shape rigid body hydrodynamics module (Sandberg 2014) is integrated via a Java Native Interface (JNI).

A scene is a description of the inner proprieties (here, Young's modulus, density, position of centre of gravity etc.) of the simulated objects (actor in Figure 2), how they are connected and, if applicable, by which plug-in they are controlled. A plug-in is a logical unit subscribing to outputs of some actors and commanding the inputs of other actors.

3.3 Control System Data Flow and Cost Model

The control system subscribes to the position of the rig and commands the necessary thrust and winch speeds to position the rig within the required watch circle. The accuracy criterion of the positioning system is a 14 m radius safety zone above the BOP, or 3.5% of the depth (NORSOK 2015). The physics engine calculates the position of the rig, the paid-out length of the rope elements, combining this with the increase in rope length due to stretch. Each winch logger subscribes to a winch and logs its inner state. The cost logger subscribes to the rig, the thruster, and the environment. The data is logged at 1Hz. Figure 3 represents the data flow between the objects. To determine the current state, the position control system subscribes to the winches, the thruster, and the rig (1). Then it sends the commands to the winches and thruster (2). They forward these commands to the physics engine (3). It dynamically calculates forces, acceleration, velocity, and position and orientation of the objects in the simulation and updates the states (4). The rich environmental scenario is the responsibility of the weather plug-in, which updates the state of the environment (2). This state is converted into commands to the physics engine (3). The cycle is repeated during the entire simulation at 20Hz.

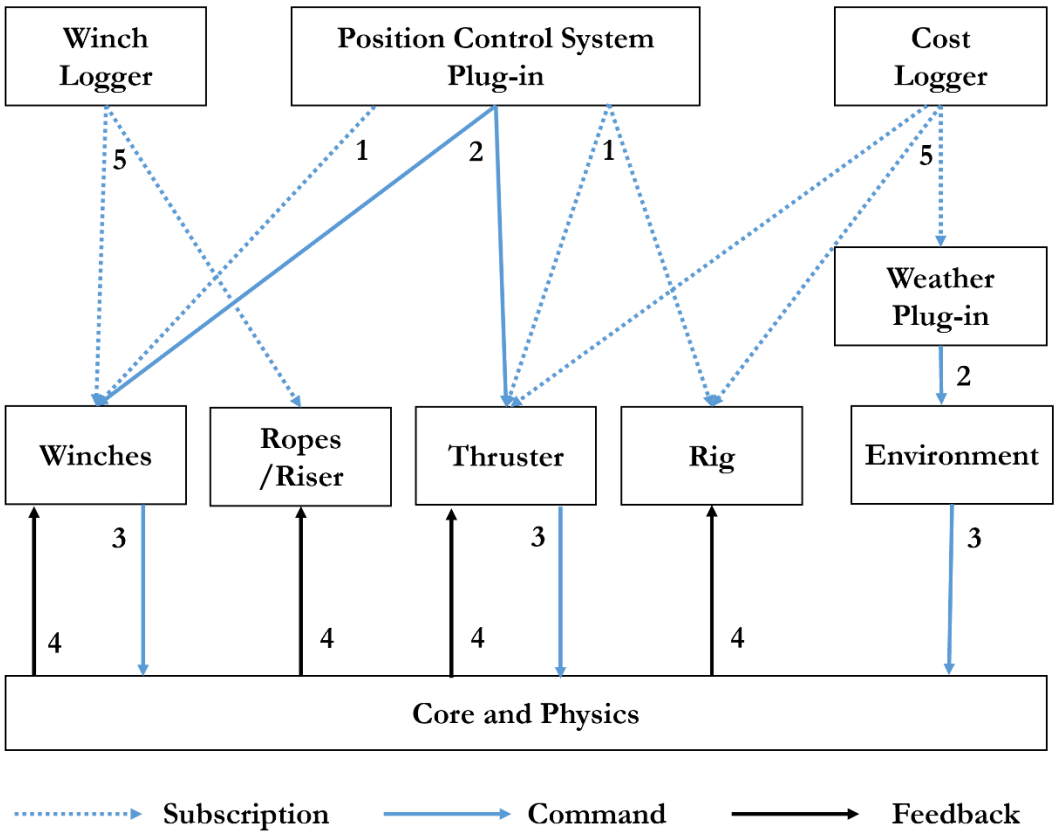

Figure 3. Schematic representation of the data flow.

The instantaneous power, $P(t)$ delivered by the thruster, is calculated by a linear approximation of the thrust-power curve (Bollard Pull of 696.61kN at 4MW), which overestimates the consumed power at low thrust. Supposing a relatively constant power between sampling intervals, the average energy E_T needed by the thruster to perform the work during this interval Δt is described in Equation 1.

$$E_T(t) = P(t) \cdot \Delta t \tag{1}$$

The whole propulsion system's efficiency η from the engine to the thruster is assumed to be 0.3, which is very optimistic. Other simulation values relevant for calculating the emissions and costs are listed in Table 1. The energy consumed by the engine is $E_T = \eta . E_E$. The Mass of MDO burned by the engine is expressed in Equation 2:

$$M_{Oil} = \frac{E_E}{E_{Oil}} = \frac{E_T}{E_{Oil}.\eta} = \frac{P(t) \cdot \Delta t}{E_{Oil} \cdot \eta} \quad (2)$$

$$M_{CO_2} = M_{Oil} \cdot F_{CO_2} = \frac{P(t) \cdot \Delta t \cdot F_{CO_2}}{E_{Oil} \cdot \eta} \quad (3)$$

$$M_{NO_x} = M_{Oil} \cdot F_{CO_2} = \frac{P(t) \cdot \Delta t \cdot F_{NO_x}}{E_{Oil} \cdot \eta} \quad (4)$$

$$T_{cost} = M_{Oil} \cdot \mathrm{C} \quad (5)$$

Table 1 . Model Values

Variable	Value	Unit	Source
C	520 (μ,σ) =(533,37)	$/T	(BunkerIndex 2017)
σ	35	GPa	(Dyneema 2018)
η	0.3		
F_{CO_2}	3.170	T/T	(EC 2002)
F_{NO_x}	50	kg/T	(NHO 2015)

It is assumed that the propulsion system consumes much more power than the winches, since, during operations, the winches pull when the ropes are slack. Therefore, the energy consumed by the winches is ignored.

3.4 Environment

The comprehensive Metocean report from the Barents Sea Exploration Collaboration (BaSec 2015) of the D-Block (73.39º N, 33.00º E, 393m over sea bed) has been summarised to give a time distribution of the environmental conditions during the May-September safe production period, then rotated according to the platform north, such that its heading faces most of the weather. A constant current velocity corresponding to its maximum value during the period has thus been set at 0.44 m/s. The wind is modelled with a timely constant and spatially uniform speed within one weather case,

and there is no gust nor shadow effect.

The irregular seas are modelled using a 60 components JONSWAP spectrum for a given sea state. The elevation at time t and point $\vec{x}$ is described in equation 9.

$$h(\vec{x}, t) = \sum_{i=1}^{60} A_i \sin(\omega_i t - \vec{k}_i . \vec{x} + \varphi_i) \tag{6}$$

Figure 1 shows the corresponding height map in the physics visualization and the Unity-based visualization. Transitions between sea states, smoothed out using time cross-fading between start state 's' and end state 'e', are modelled as detailed in equation 7. The weather model does not include extreme weather values in order to reflect the normal operation during production, not the survival capabilities of the rig.

$$h(\vec{x}, t) = \big(1 - \alpha(t)\big) \sum_{i=1}^{60} A_{i,e} \sin\big(\omega_{i,e} t - \vec{k}_{i,e} . \vec{x} + \varphi_{i,e}\big) + \alpha(t) \sum_{i=1}^{60} A_{i,s} \sin\big(\omega_{i,s} t - \vec{k}_{i,s} . \vec{x} + \varphi_{i,s}\big) \tag{7}$$

Table 2. May-September Weather Distribution by Platform North Sectors

Hs [m]	Wind Vel. [m/s]	0 º	30 º	60 º	90 º	120 º	150 º	180 º	210 º	240 º	270 º	300 º	330 º	%
1	5	2.404	2.213	1.993	1.861	1.995	2.217	2.322	2.382	2.378	2.448	2.348	2.426	26.99
2	10	5.907	5.418	3.878	2.918	3.313	4.164	4.633	4.609	4.687	4.363	4.333	4.771	79.98
3	15	2.188	1.893	0.859	0.450	0.811	1.002	1.167	1.075	1.205	0.945	1.024	1.503	94.11
4	15	0.620	0.536	0.243	0.127	0.230	0.284	0.330	0.304	0.341	0.267	0.290	0.426	98.10
5	20	0.257	0.109	0.030	0.044	0.095	0.138	0.137	0.137	0.069	0.106	0.113	0.132	99.47
6	20	0.062	0.026	0.007	0.011	0.023	0.033	0.033	0.033	0.017	0.026	0.027	0.032	99.80
7	25	0.017	0.000	0.000	0.000	0.015	0.017	0.020	0.050	0.020	0.030	0.020	0.010	100.00

3.5 Ropes

HMPE ropes made from Dyneema® fiber DM20 XBO have ultra-low creep and

prolonged bending life. They keep their physical properties over many work cycles. HMPE ropes have a static and a dynamic stiffness, while both terms decrease with temperature the later increases with excitation frequency and is therefore non-linear. Based on (Vlasblom et al. 2012), only linear effects are considered. The static stiffness is set at a Young's stretch modulus σ of 35 GPa, which is rather low. This constitutes a conservative approach that underestimates the static mode's capability of staying in the watch circle. Using Young's formula to derive the rope's elongation ΔL in Equation 8, with L length of the rope, F the mooring tension (after pre-tensioning), D the diameter for the line yields this equation:

$$\Delta L = \frac{4FL}{\pi D^2 \sigma} \tag{8}$$

Since mooring winches of 76mm diameter steel wires are already installed on Island Innovator, the wires are replaced by with ropes of the same dimension, simplifying retrofit. Using L = 620m and F = 2450kN yields an elongation of 9.6 m, which gives an indication that such rope diameter might be inappropriate for conventional static mooring. However, one of the motivations of this VP study is to show that an active mooring winch control algorithm can mitigate this weakness. This algorithm is presented in the next subsections.

3.6 Modes

The three modes sketched in Figure 4, are as follows:

- **Active Mode:** Only four winches with a maximum pull-in force of 1471kN

- **DP Mode:** Six 4 MW thrusters are modelled as one perfect 24 MW Azimuth Thruster, without thrust or angular ramping time. Because one thruster is not enough to apply a righting moment, for the sake of simplification of the thrust allocation algorithm, the winches are set to hold a break force of 294kN to prevent the platform from rotating around the vertical axis.
- **AHP-K Mode:** The winches are working as they do in active mode, and the DP is activated to complement the winches when necessary.

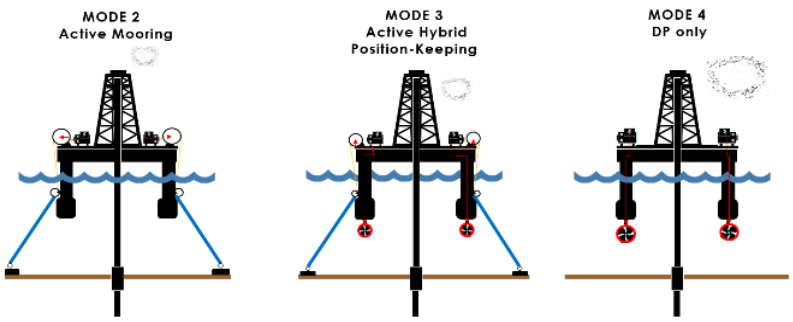

Figure 4. Schematics of the positioning modes. Courtesy of Deep Tek.

3.7 Control Algorithms

Figure 5 shows the layout of the winches (triangles), suction anchors (small circles) and the rig (bold square). The winches have limited pay-in/out speed (1 m/s) and acceleration (1 m/s^2), but no such physical constraints were applied to the thruster.

Figure 6 shows the modes as decisions in the top of the flow chart (tilted squares). Proportional integral derivative (PID) regulators are applied in the three control modes to generate speed commands for winch actuators, and angle and magnitude commands

for the azimuth thruster. The position error is selected as the input signal for all three control modes:

$$\boldsymbol{e}_p = \boldsymbol{p}_B - \boldsymbol{p}_A \tag{9}$$

, where $\boldsymbol{p}_A$ is the current horizontal position and $\boldsymbol{p}_B$ is the desired horizontal position, marked as "A" and "B" in Figure 5 (right). Figure 6 shows the processes used for each mode. These will be described in more detail in the subsequent paragraphs.

In both "Active" and "AHP-K" modes, two of the four winches work actively using PID regulators to reduce the position error of the rig at any given time. This means they will haul in to pull the rig towards the target. The other two winches are under control of a constant tension controller, such that they pay in/out to keep ropes on the lee side (e.g., winches 1 and 2 in Figure 5) tight within an acceptable tension.

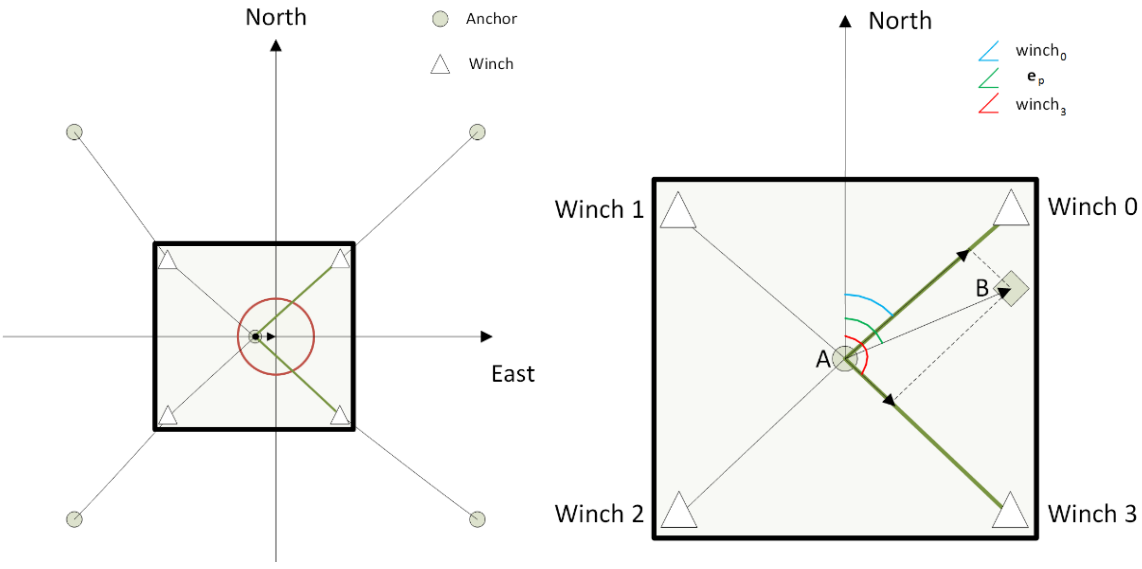

Figure 5. Overhead view of the rig and its winch and anchor layout. The red circle exemplifies the threshold for engaging the thruster in AHP-K mode (left). Zoomed view of the rig, its winches, the current position (A) and the desired position (B) (right)

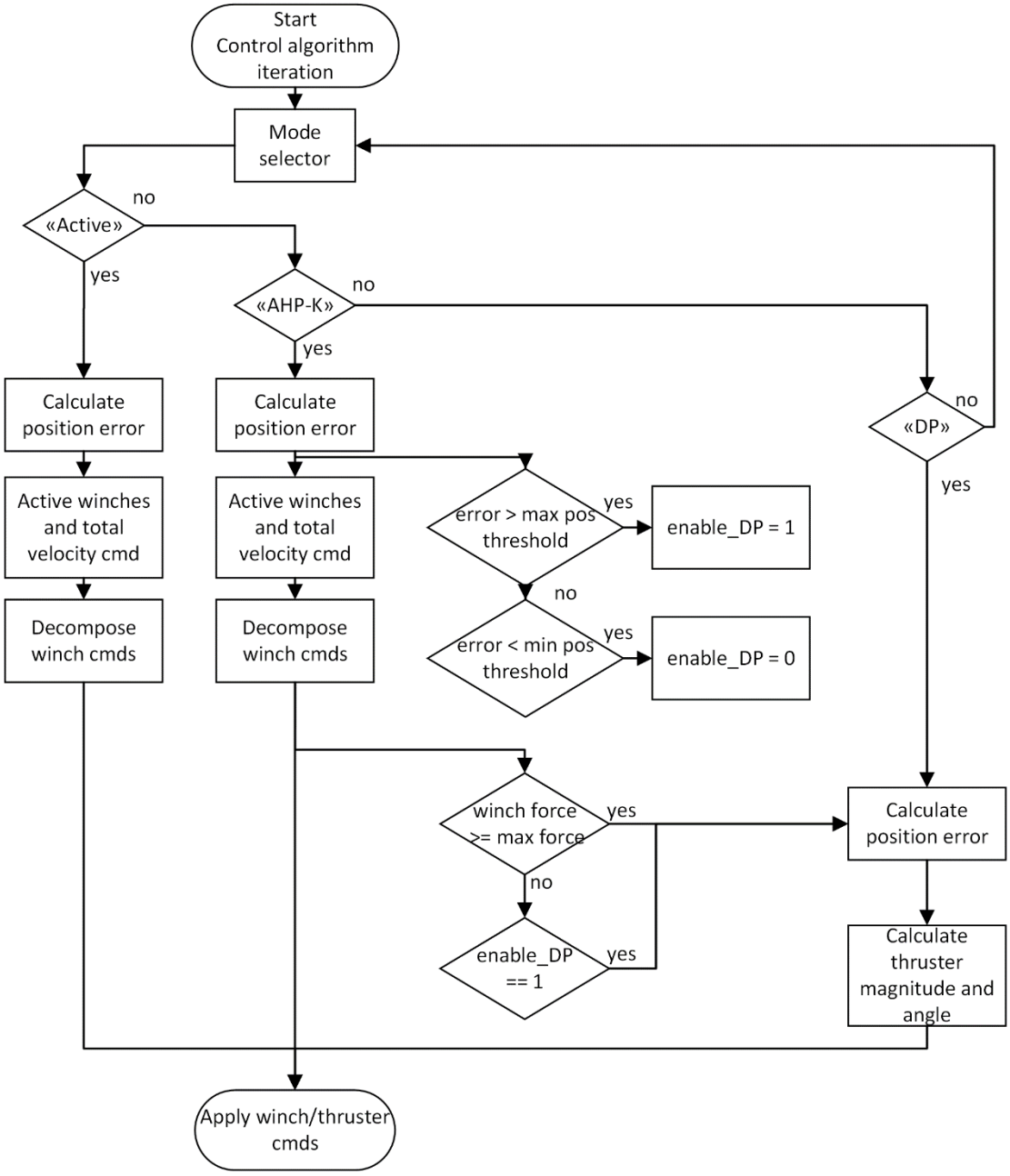

Figure 6. A view of the logic contained in one iteration of the control algorithm.

The PID output command of the active winch mode is a vector that specifies the commanded force in the North and East direction in order to converge on the desired position. The length of this vector, scaled by a force-to-winch-speed factor, becomes the desired total speed as if a single winch was pulling along the line spanning the points A-B of Figure 5:

$$\mathbf{u}_{\mathrm{tot}} = \mathrm{k}_1 \times \mathrm{PID}(\mathbf{e}_{\mathrm{p}}) \tag{10}$$

PID is a function that takes the position error vector ($\boldsymbol{e}_p$) and outputs a north and east winch force component. A further transformation is required before issuing winch speed commands, meaning $\boldsymbol{u}_{tot}$ must be projected along the pulling directions of the two winches. Taking Figure 5 as an example, where the rig is located west of its desired position, the decomposed speed commands are shown in equations 11 and 12. The decomposition is visualised in Figure 5, as arrows along the green lines from the centre of the rig to winch 0 and 3.

$$u_{winch_0} = cos\big(\angle \boldsymbol{e}_p - \angle winch_0\big) \times ||\boldsymbol{u}_{tot}||_2 \tag{11}$$

$$u_{winch_3} = cos\big(\angle \boldsymbol{e}_p - \angle winch_3\big) \times ||\boldsymbol{u}_{tot}||_2 \tag{12}$$

A more straightforward approach is taken for the DP control mode. By employing a different set of PID parameters, the position is directly transformed into a force vector. The azimuth angle of the thruster is determined by the direction of the force vector and the magnitude is the length of the vector.

When AHP-K mode is active, the thruster runs in parallel to the winches if either of these conditions hold:

- The position error exceeds 2 m, called “pos threshold” in Figure 6;
- The force measured at one or more winches reaches the limit of 1471kN, called “max force” in Figure 6.

When the rig re-enters its desired position, such as within a 5 cm radius of its original position, the thruster is deactivated, leaving the position control task to the winches. Such a low threshold for disusing the thruster when in the AHP-K mode may cause excessive power consumption. To smooth the jumps in commanded thruster force due to the DP activation/deactivation, a linear transition of the PID parameters was performed.

4 Simulation Results

Presented in Figure 7 and Figure 8 and summarised in Table 3, the simulation results show that Active mode can hold the rig in position for significant wave heights up to 3m and wind speeds up to 15 m/s, representing almost 80% of the weather as shown in the last column of Table 2. DP mode holds the rig until the wind speed reaches 20m/s and the significant wave height of 6m. AHP-K mode holds the rig in position in any representative sea state. In the 20-25m/s cases, the DP-controlled thruster prevails in AHP-K mode. However, the active winches help smooth out the peaks, as seen at the end of the run, after 30000s in Figure 7. In other terms, while neither DP nor Active Mooring modes can hold the rig in position, the combination of both can. This is because AHP-K because has more actuators to rely upon.

In AHP-K mode, the thruster does not significantly start before the wind velocity is 15 m/s and significant wave height is 4 m. This corresponds to 98% of the weather during the drilling season (Table 2). When excluding the transitions between the sea states, the financial costs and gas emissions of AHP-K mode are 72.6% lower than DP

mode, and the thruster is active 70% less. This results in an equal reduction in time spent generating thruster-induced underwater noise.

Table 3. Summary of the costs, emissions, and positioning performance

Cost	Unit	Active	AHP-K	DP
MDO	[T]	0	0.96	3.52
T_{cost} (5)	[$]	0	502	1830
CO_2	[T]	0	3.06	11.16
NO_x	[kg]	0	48	176
Maximum Offset	[m]	150.78	11.52	38.84
Seconds with Active Thruster		0	2173	7244
Holds until Wind Speed/ Wave Height	[m/s]/ [m]	15/3	25/7	20/6

The control systems of all three modes were based on simple PID algorithms, which could be improved to be more adaptive to the environmental conditions by including for instance a feedforward gain to counteract mean wind forces (Fossen 2011). Even if the DP and winch algorithms do not have knowledge of each other, the study did not find obvious cases of overshooting in which DP and winches overcompensate for the weather. The extreme offset peaks in the DP mode in Figure 7 can be imputed to different factors:

- Lack of righting moment of the thruster to set the rig in the most favourable heading winch positions and orientations on the rig.
- Lag induced by the low-pass filter in addition to PID parameters that are not aggressive causes a slow response to position error
- Collinearity of wind and waves in unfavourable directions

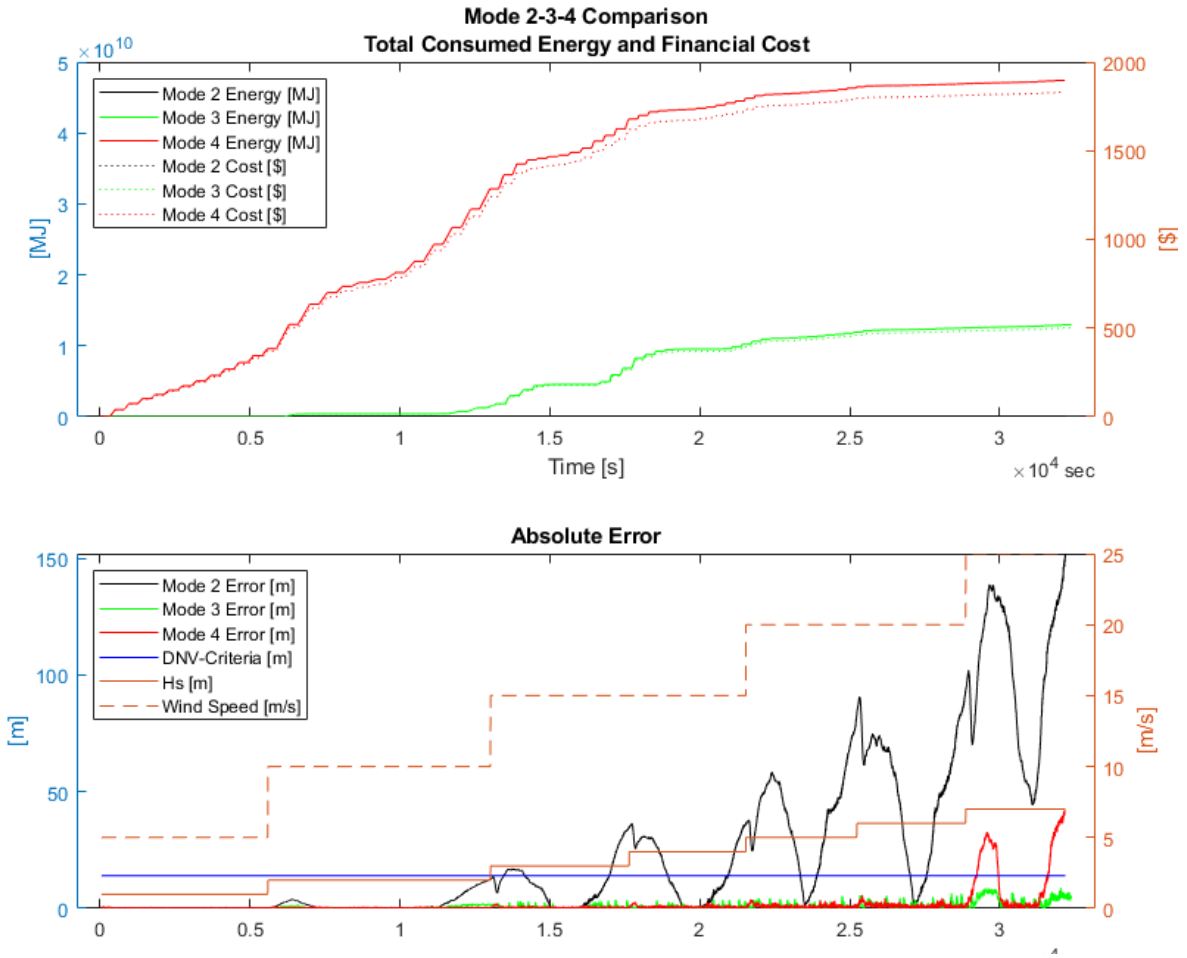

Figure 7. Comparison of the energy/cost (top) and position performance in varying wave/wind conditions (bottom).

It remains to study what the weaknesses of the Active Mode are to be imputed to: the simplistic approach of the control algorithm or the winch configuration. The latter depends on engineering decisions that were out of the scope of the study, such as:

- Number of winches (4 or 8)
- Winch positions and orientations on the rig.
- Thickness of the rope (76mm or thicker)
- Maximum winch pulling force (1471kN or more).

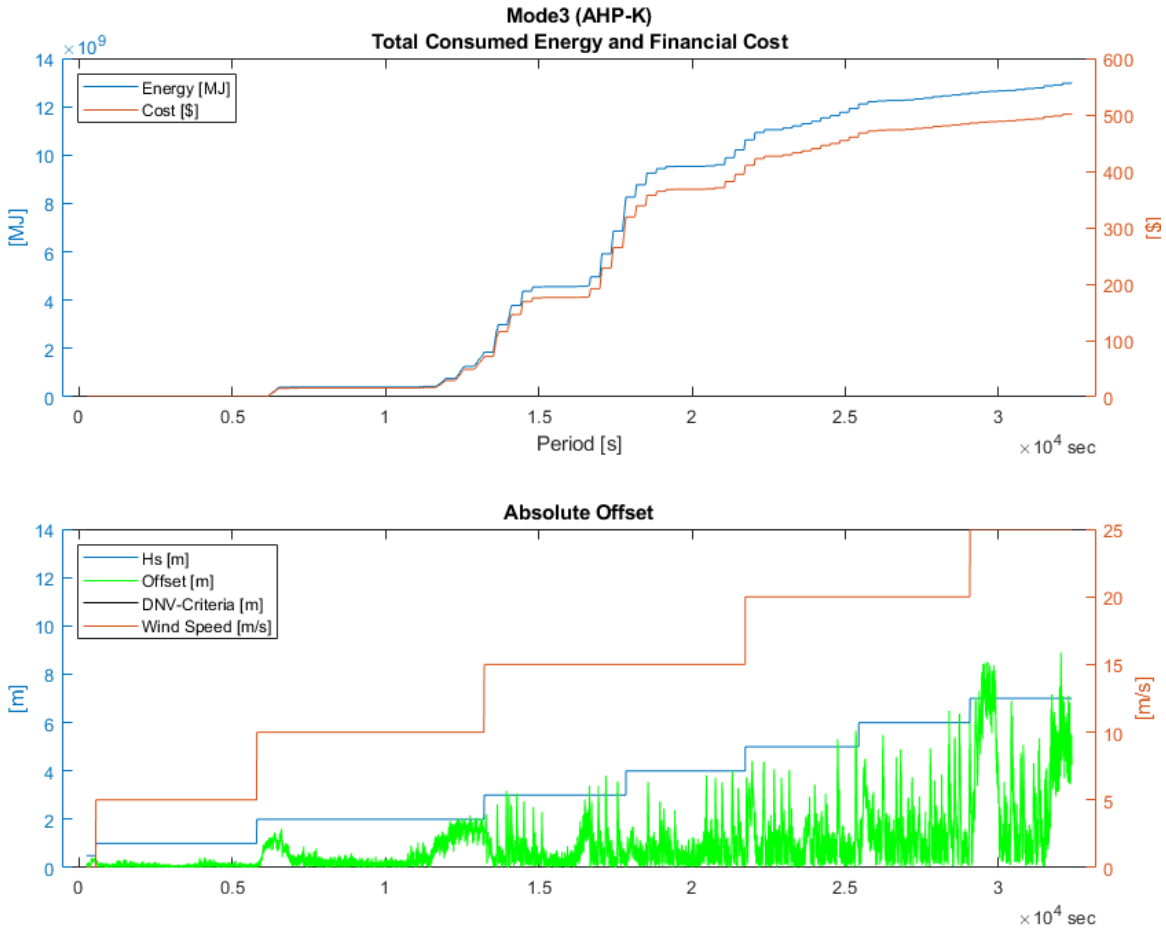

Figure 8.Cost and energy consumption (top) and position performance in varying wave/wind conditions for the AHP-K mode.

5 Conclusions

This study establishes the VP simulation of an innovative and potentially cost-saving mooring system. First the original physical system to be simulated is virtually built using 3D meshes, ropes, winches, anchors, and a thruster. Secondly, plug-ins are added to the simulation. One external plug-in dynamically commands the winches and thruster

responses. One internal plug-in controls the rich environment composed of multi-directional JONSWAP spectrum, wind, and current. The simulation setup is proven appropriate for VP and testing position-keeping systems. This allows to simulate an AHP-K, a novel rig positioning system which dynamically pays winches in and out and activates and deactivates the thruster to reposition the rig in the desired watch circle while minimizing the operating costs.

In the special case of a rig operating in the Barents Sea during the summer period, the use of DP-controlled thrusters could be avoided at least 70% of the time, reducing underwater noise by the same amount, thereby facilitating significant energy and gas emission savings of up to 72.6%. The software VP platform shows good consistency between the different modelled solutions.

This study validates VP as an exploration tool of the engineering design space: further studies will address the user-friendliness and speed of VP process and explore rope diameter, number of winches and thrusters, and improved control algorithms.

6 Acknowledgements

The Norwegian Research Council supported this work under Grant 255959; RRFMidt Norge supported it under Grant 274104; Deep Tek AS, DSM, and Offshore Simulator Centre.

7 References

Aamo O.M., Fossen T.I. 1999. Controlling line tension in thruster assisted mooring systems, IEEE Conference on Control Algorithms, Proceedings, Volume 2, 1999, p. 1104-1109.

Algoryx. 2018. https://www.algoryx.se [Accessed October 3rd, 2018]

BaSec. 2015. Barents Sea Exploration Collaboration, ME2015_005

BunkerIndex. 2017. https://bunkerindex.com/prices/ [Accessed September 1st, 2017]

Chu Y, Hatledal, L.I., Zhang H, Æsøy V and Ehlers S. 2017. Virtual Prototyping for Maritime Crane Design and Operations, Journal of Marine Science and Technology.

DNVGL. 2018. https://www.dnvgl.com/Images/Sesam-Feature-Description_tcm8-58834.pdf [Accessed December 16th, 2018]

Dyneema. 2019. www.dsm.com [Accessed March 7th, 2019]

European Commission. 2002. Quantification of emission from ships http://ec.europa.eu/environment/air/pdf/chapter3_end_ship_emissions.pdf [Accessed 2018 Oct 03]

Fossen, T.I, 2011. Handbook of Marine Craft Hydrodynamics and Motion Control. Handbook of Marine Craft Hydrodynamics and Motion Control. Trondheim.Wiley.

Ha S, Ku N, Roh MI. 2016. Event-based scenario manager for multibody dynamics simulation of heavy load lifting operations in shipyards. International Journal of Naval Architecture and Ocean Oceaneering, Volume 8, Issue 1, January 2016, p. 83-101.

Island Drilling. 2018. http://www.islanddrilling.no/bilder/filer/ IslandInnovator.pdf [Accessed October 3rd, 2018]

Ji S-W, Choi M-S, and Kim Y-B. 2015. A Study on Position Mooring System Design for the Vessel Moored by Mooring Lines, IEEE/ASME transactions on mechatronics, vol. 20, no. 6, December 2015

Kim Y. 2014. A study on the control system design for ship mooring winch system, Journal of Mechanical Science and Technology, 28(3), p. 1065–1072.

Leite S, Boesten J. 2011. HMPE Mooring Lines for Deepwater MODUs. Offshore Technology Conference, OTC 22486

Li G, Skogeng PB, Deng Y, Hatledal LI, and Zhang H. 2016. Towards a virtual prototyping framework for ship maneuvering in offshore operations. In IEEE OCEANS 2016-Shanghai, p. 1-6

NPD. 2017. Norwegian Petroleum Directorate, Resource Accounts http://www.npd.no/en/Topics/Resource-accounts-and--analysis/Temaartikler/Resource-accounts/2017/ [Accessed October 3rd, 2018]

NORSOK U001 WELL SYSTEM LOADS NORSOK U001. 2015. Well System loads

Næringlivet Hovedorganisajon (NHO). 2015. www.nho.no/Prosjekter-og-programmer/NOx-fondet/The-NOx-fund/News/20151/new-factors-for-standard-value/ [Accessed 2018 May 17]

OrcaFlex. 2018. [Accessed 2018 December 16]. https://www.orcina.com

Reite KJ, Føre M, Aarsæther KG, Jensen J, Rundtop P, Kyllingstad L, Endresen PC, Kristiansen D, Johansen V, Fredheim. 2014. FHSIM — Time Domain Simulation of Marine Systems, Proceedings of the ASME, 2014, 33rd International Conference on Ocean, Offshore and Arctic Engineering, OMAE 2014, June 8-13, 2014, San Francisco, California, USA

Salvesen N, Tuck E.O, Faltinsen O. 1970. Ship motions and sea loads. In Transactions of the Society of Naval Architects and Marine Engineers, vol. 78, p. 250– 287

Sandberg S. 2014. Interactive Simulation of Hydrodynamics of Arbitrary Shapes, http://www.diva-portal.org/smash/record.jsf?pid=diva2%3A725897&dswid=-147

Sha Y, Amdahl J, Aalberg A, Yu Z. 2018. Numerical investigations of the dynamic response of a floating bridge under environmental loadings, Ships and Offshore Structures, 13:sup1, p. 113-126

ShipX. 2018. https://www.sintef.no/en/software/shipx. [Accessed December 16th, 2018]

Vlasblom M, Boesten J, Leite S, Davies P. 2012. Creep and Stiffness of HMPE Fiber for Permanent Deepwater Offshore Mooring, Oceans Yeosu

Wamit. 2018. http://www.wamit.com. [Accessed December 16th, 2018]

Williams R, Wright AJ, Ashe E, Blight LK, Bruintjes R, Canessa R, Clark CW, Cullis-Suzuki S, Dakini DT, Erbe C, Hammond PS, et al. 2015. Impacts of anthropogenic noise on marine life: Publication patterns, new discoveries, and future directions in research and management. Ocean & Coastal Management, Volume 115, October 2015, p. 17-24

Yu Y, Duan M, Sun C, Zhong Z, Liu H. 2017. A virtual reality simulation for coordination and interaction based on dynamics calculation, Ships and Offshore Structures, 12:6, p. 873-884

Zhang X, Duan M, Mao D, Yu Y, Yu J & Wang Y. 2017. A mathematical model of virtual simulation for deepwater installation of subsea production facilities, Ships and Offshore Structures, 12:2, p.182-195

List of Tables

Table 3 . Model Values

Variable	Value	Unit	Source
C	520 (μ,σ) =(533,37)	$/T	(BunkerIndex 2017)
σ	35	GPa	(Dyneema 2019)
η	0.3		
F_{CO_2}	3.170	T/T	(EC 2002)
F_{NO_x}	50	kg/T	(NHO 2015)

Table 2. May-September Weather Distribution by Platform North Sectors

Hs [m]	Wind Vel. [m/s]	0 º	30 º	60 º	90 º	120 º	150 º	180 º	210 º	240 º	270 º	300 º	330 º	%
1	5	2.404	2.213	1.993	1.861	1.995	2.217	2.322	2.382	2.378	2.448	2.348	2.426	26.99
2	10	5.907	5.418	3.878	2.918	3.313	4.164	4.633	4.609	4.687	4.363	4.333	4.771	79.98
3	15	2.188	1.893	0.859	0.450	0.811	1.002	1.167	1.075	1.205	0.945	1.024	1.503	94.11
4	15	0.620	0.536	0.243	0.127	0.230	0.284	0.330	0.304	0.341	0.267	0.290	0.426	98.10
5	20	0.257	0.109	0.030	0.044	0.095	0.138	0.137	0.137	0.069	0.106	0.113	0.132	99.47
6	20	0.062	0.026	0.007	0.011	0.023	0.033	0.033	0.033	0.017	0.026	0.027	0.032	99.80
7	25	0.017	0.000	0.000	0.000	0.015	0.017	0.020	0.050	0.020	0.030	0.020	0.010	100.00

Table 3. Summary of the costs, emissions, and positioning performance

Cost	Unit	Active	AHP-K	DP
MDO	[T]	0	0.96	3.52
T_{cost} (5)	[$]	0	502	1830
CO_2	[T]	0	3.06	11.16
NO_x	[kg]	0	48	176
Maximum Offset	[m]	150.78	11.52	38.84
Seconds with Active Thruster		0	2173	7244
Holds until Wind Speed/ Wave Height	[m/s]/ [m]	15/3	25/7	20/6

List of Figures

Figure 1

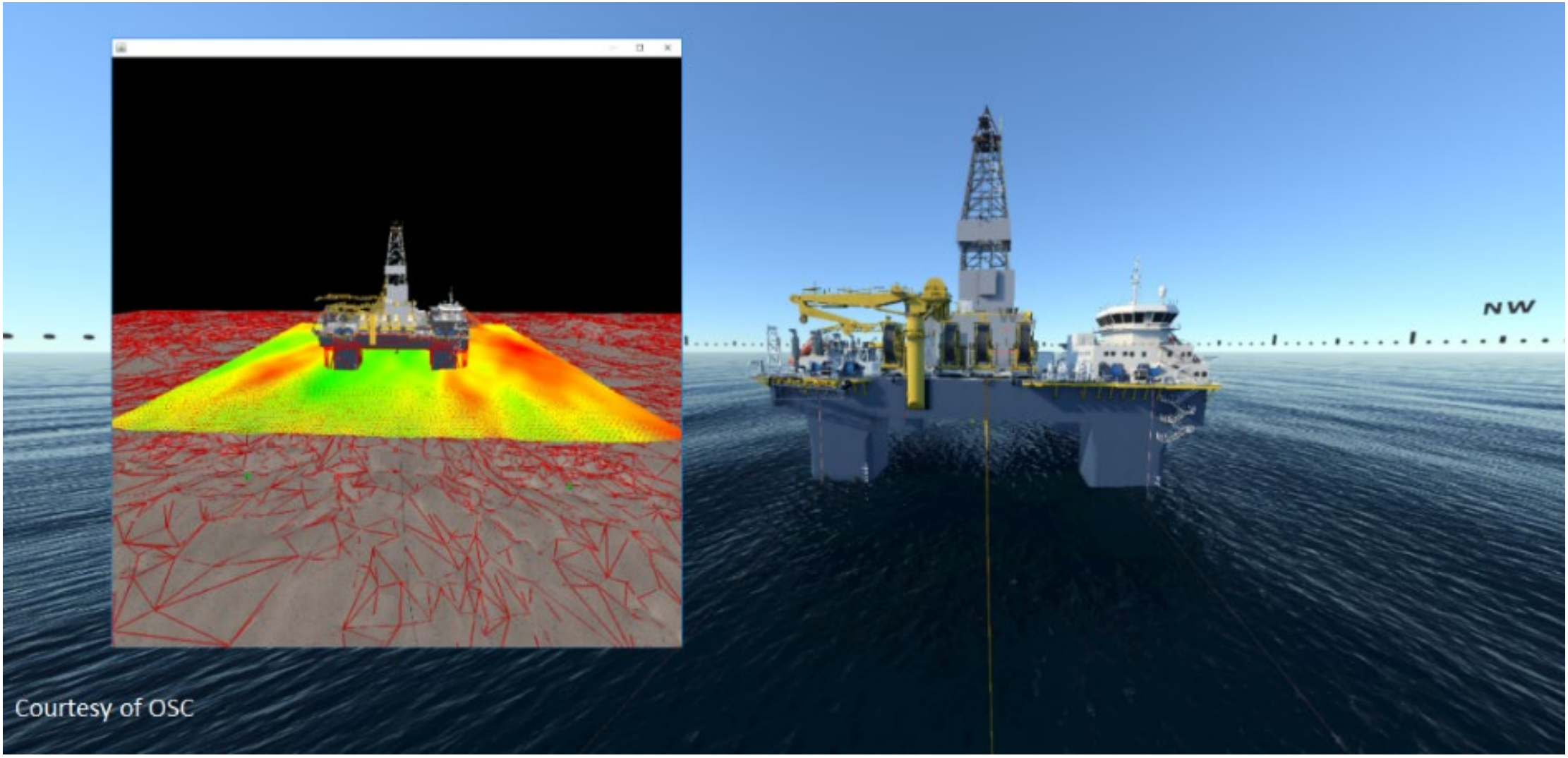

Figure 2

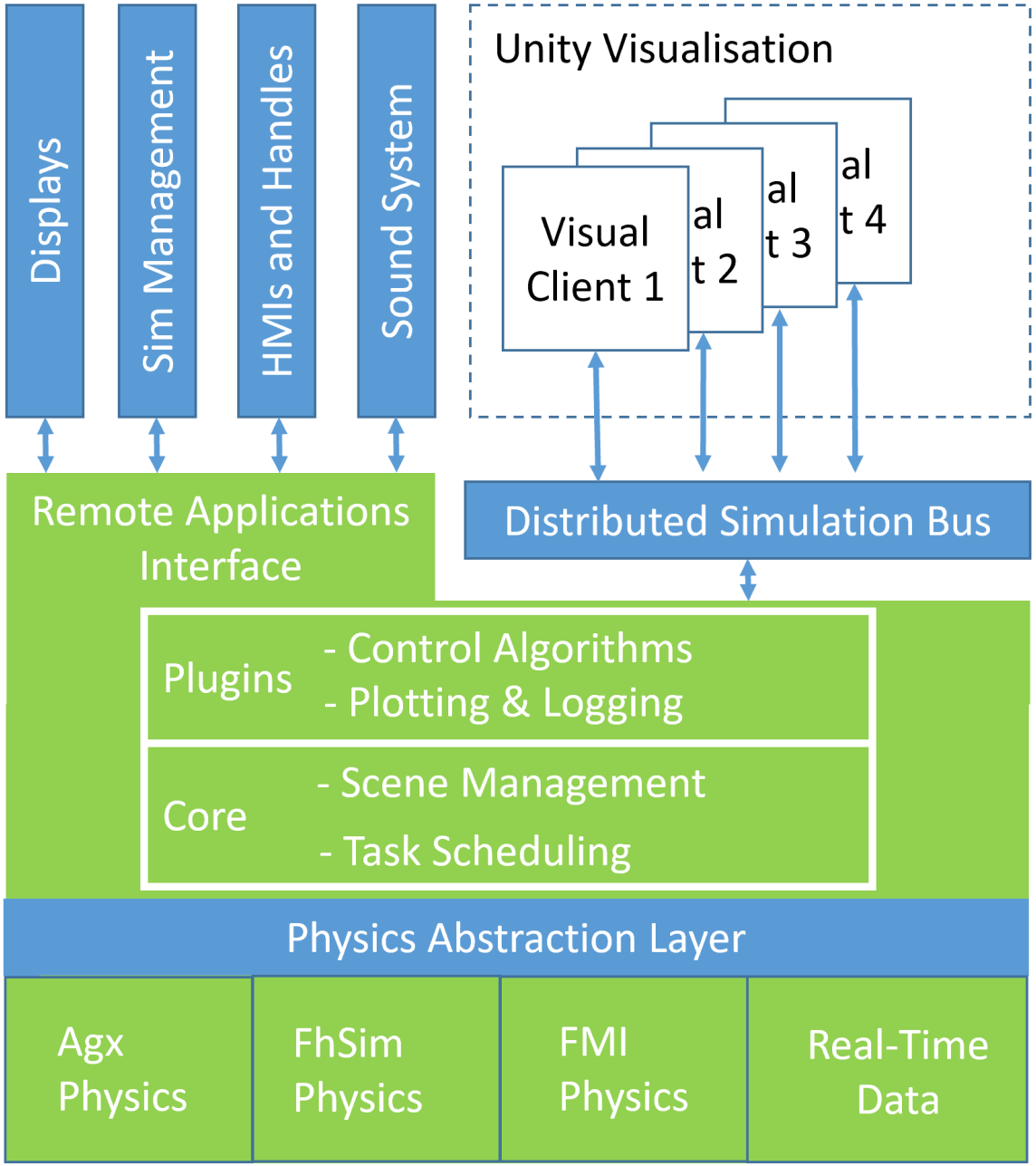
Displays
Sim Management
HMIs and Handles
Sound System
Unity Visualisation
Visual Client 1
al t 2
al t 3
al t 4
Remote Applications Interface
Distributed Simulation Bus
Plugins
- Control Algorithms
- Plotting & Logging
Core
- Scene Management
- Task Scheduling
Physics Abstraction Layer
Agx Physics
FhSim Physics
FMI Physics
Real-Time Data

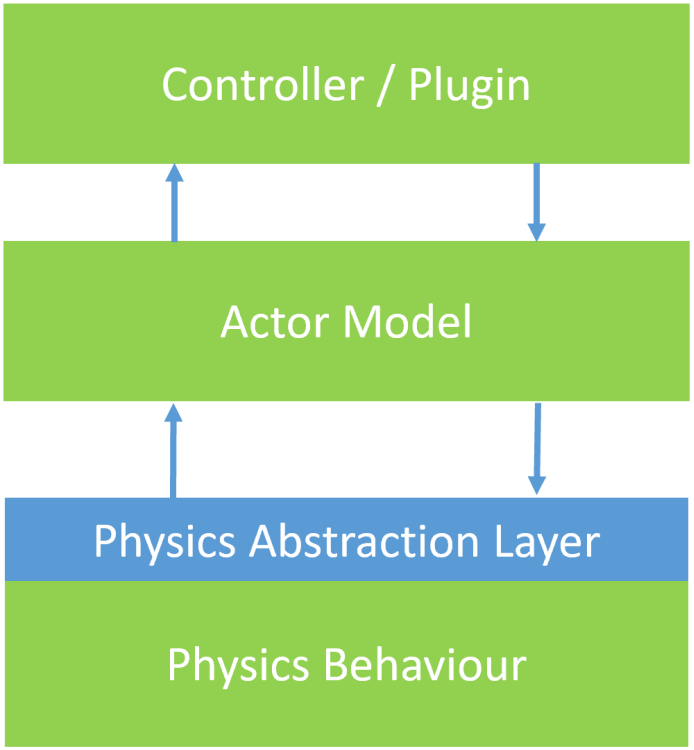
Controller / Plugin
Actor Model
Physics Abstraction Layer
Physics Behaviour

Figure 3

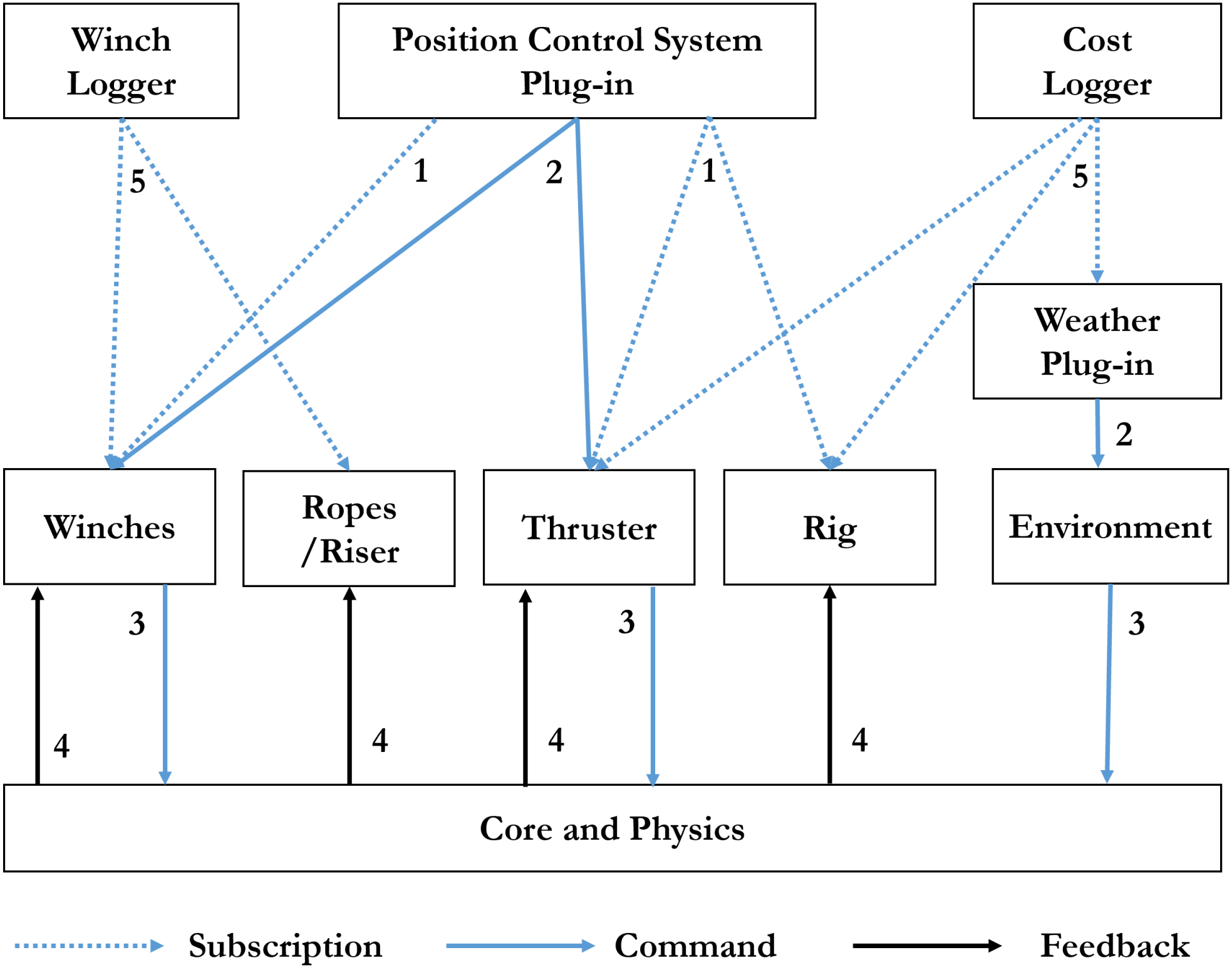
Winch Logger
Position Control System Plug-in
Cost Logger
Weather Plug-in
Winches
Ropes /Riser
Thruster
Rig
Environment
Core and Physics
1
2
1
5
5
2
3
3
3
4
4
4
4
Subscription
Command
Feedback

Figure 4

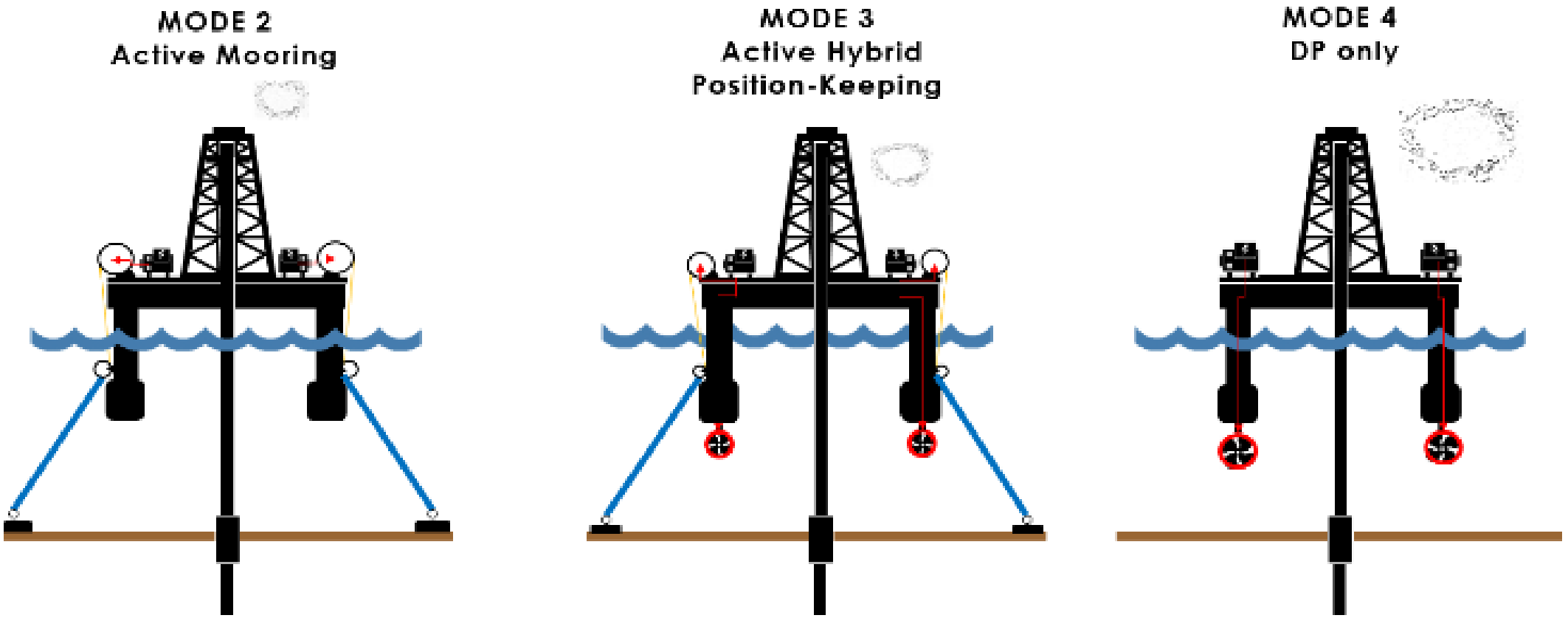
MODE 2
Active Mooring
MODE 3
Active Hybrid
Position-Keeping
MODE 4
DP only

Figure 5

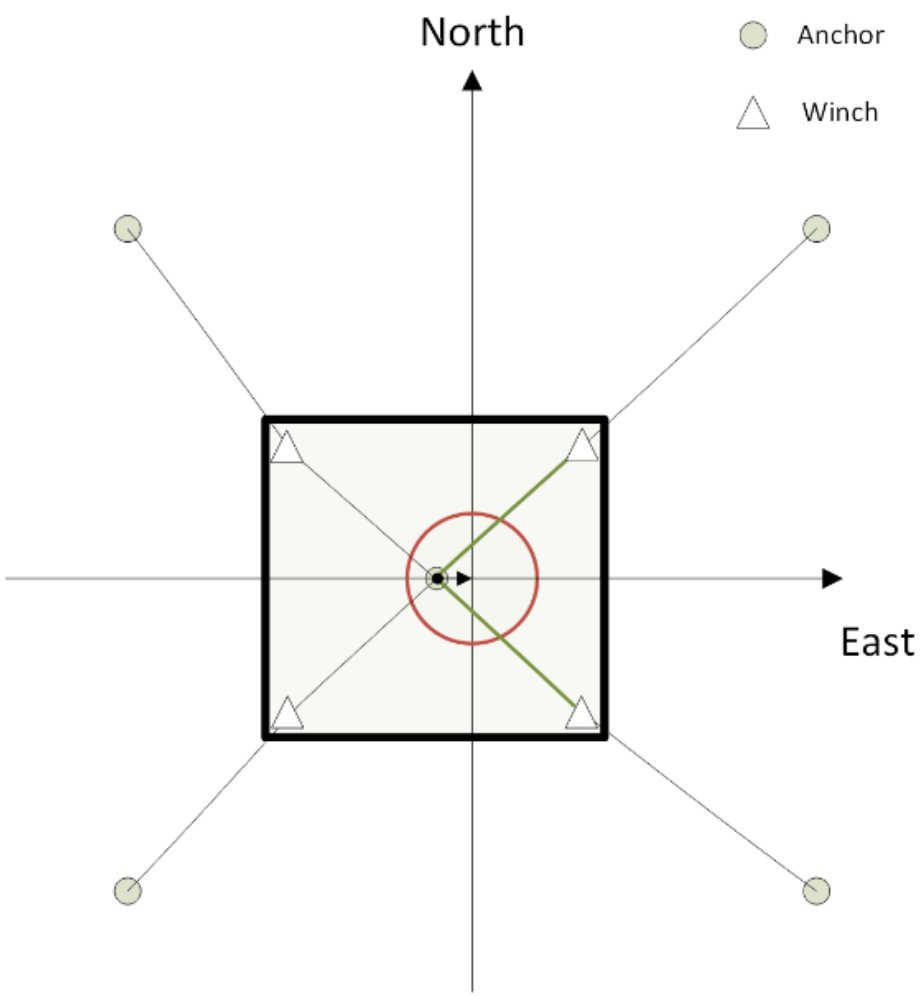
North
Anchor
Winch
East

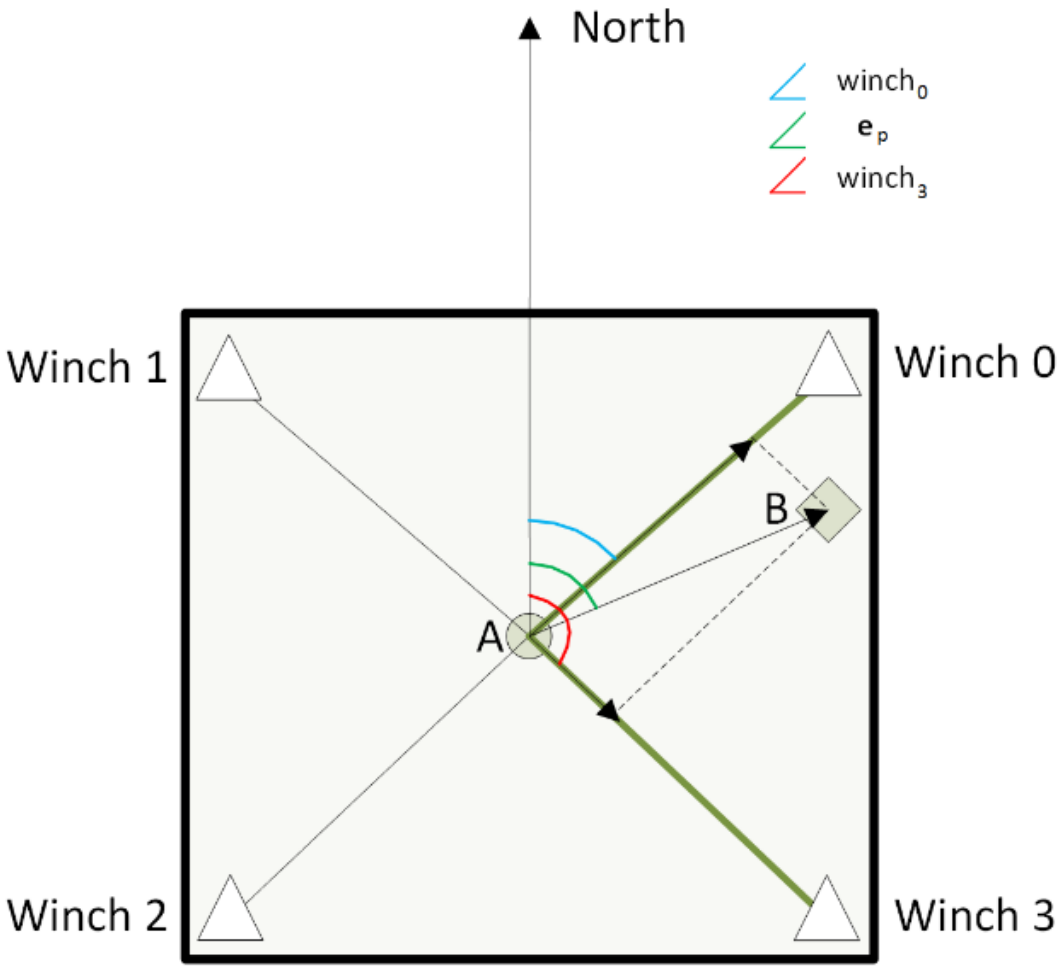
North
winch0
ep
winch3
Winch 1
Winch 0
B
A
Winch 2
Winch 3

Figure 6

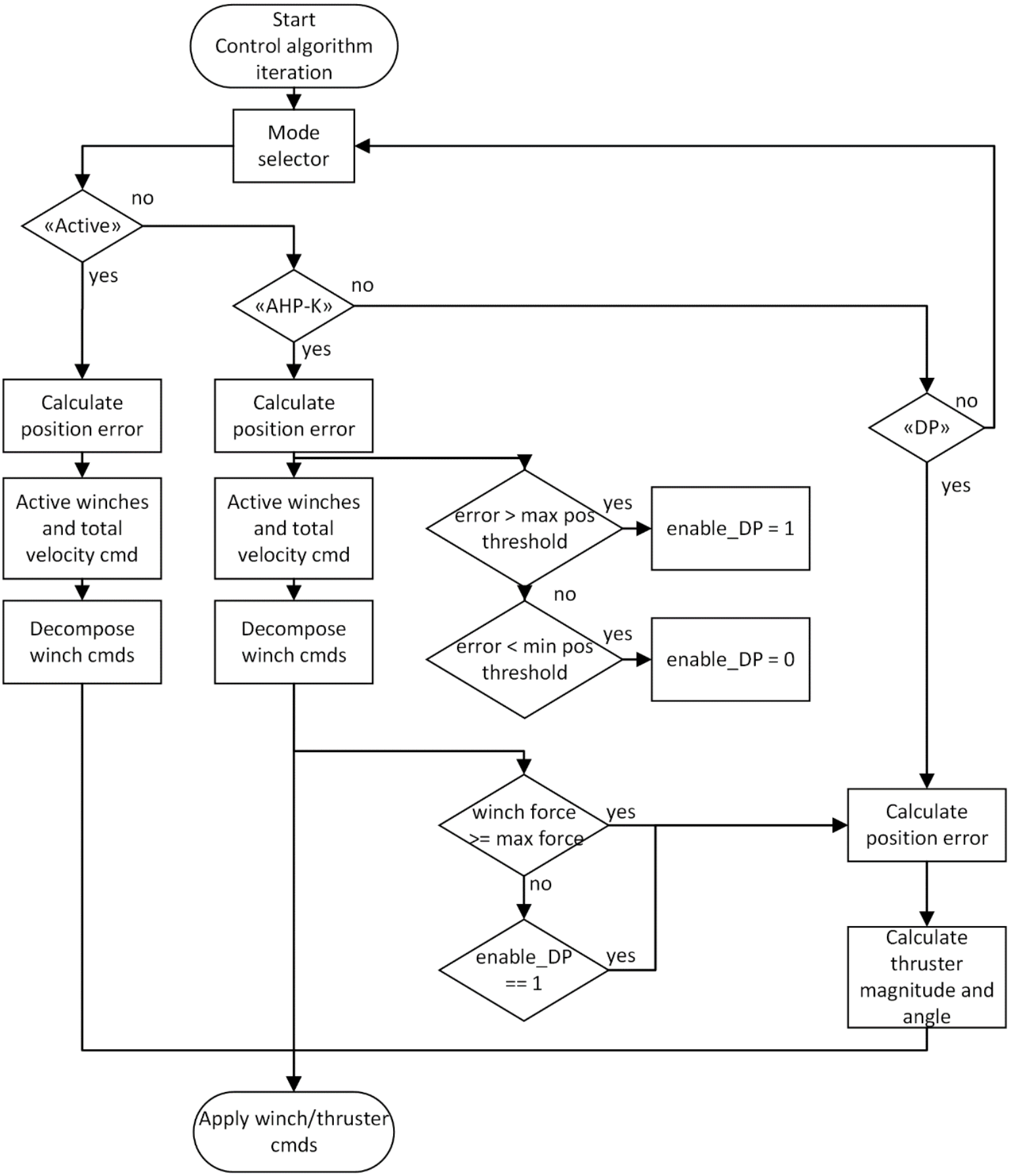
Start
Control algorithm iteration
Mode selector
«Active»
no
yes
«AHP-K»
no
yes
«DP»
no
yes
Calculate position error
Calculate position error
Active winches and total velocity cmd
Active winches and total velocity cmd
Decompose winch cmds
Decompose winch cmds
error > max pos threshold
yes
enable_DP = 1
no
error < min pos threshold
yes
enable_DP = 0
winch force >= max force
yes
no
enable_DP == 1
yes
Calculate position error
Calculate thruster magnitude and angle
Apply winch/thruster cmds

Figure 7

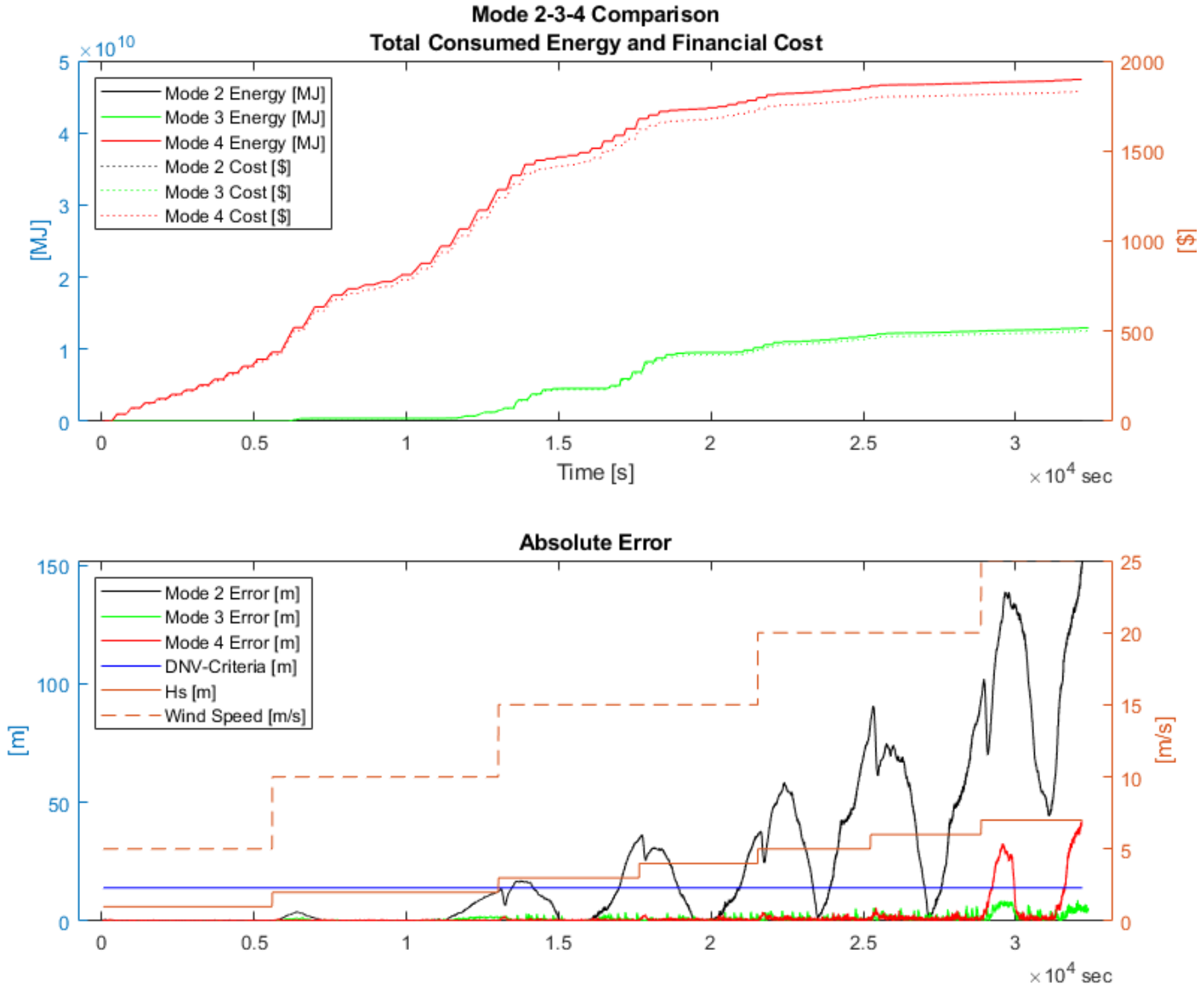
Mode 2-3-4 Comparison
Total Consumed Energy and Financial Cost
×10^10
[MJ]
[$]
Mode 2 Energy [MJ]
Mode 3 Energy [MJ]
Mode 4 Energy [MJ]
Mode 2 Cost [$]
Mode 3 Cost [$]
Mode 4 Cost [$]
Time [s]
×10^4 sec
Absolute Error
[m]
[m/s]
Mode 2 Error [m]
Mode 3 Error [m]
Mode 4 Error [m]
DNV-Criteria [m]
Hs [m]
Wind Speed [m/s]
×10^4 sec

Figure 8

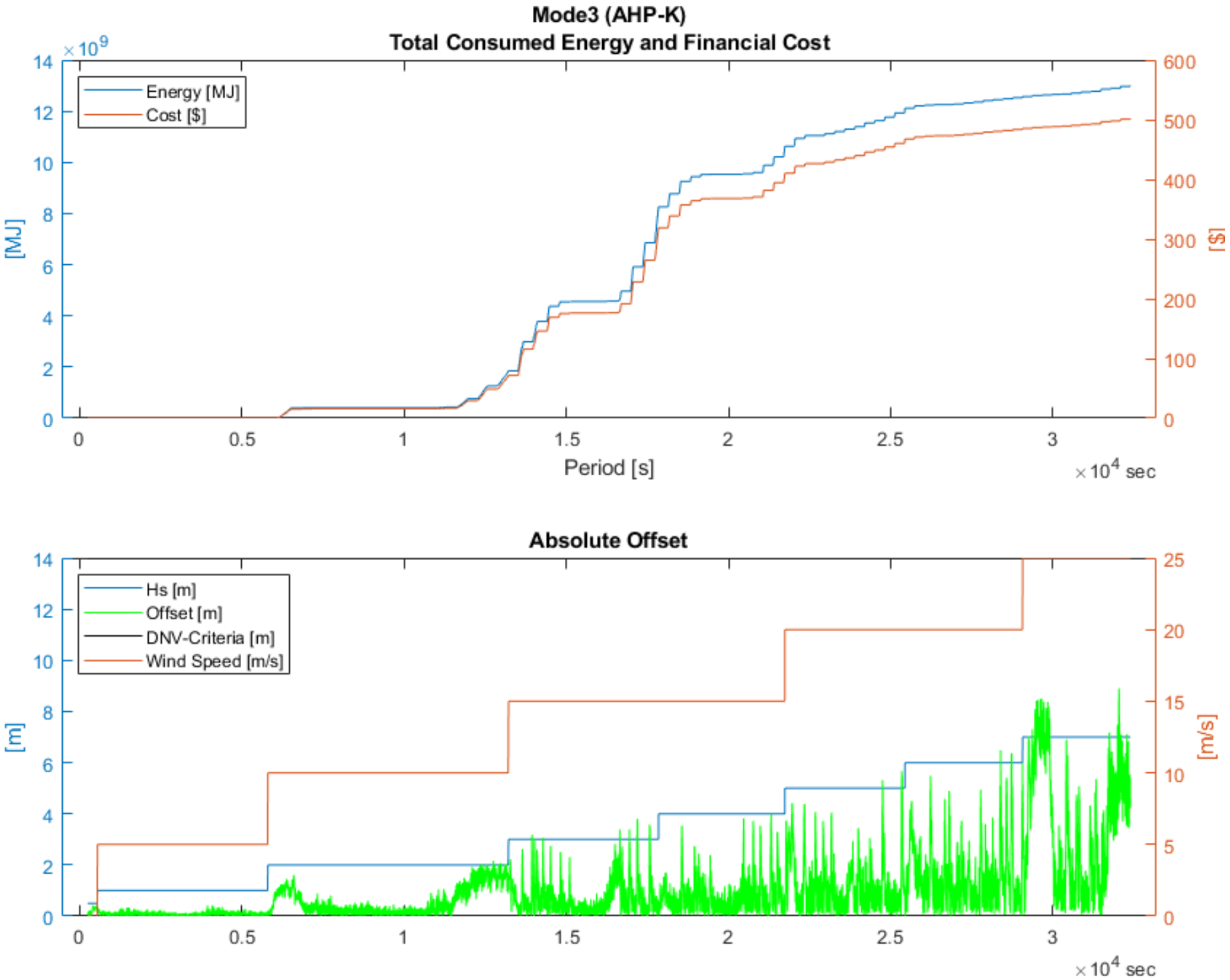
Mode3 (AHP-K)
Total Consumed Energy and Financial Cost
×10^9
Energy [MJ]
Cost [$]
[MJ]
[$]
Period [s]
×10^4 sec
Absolute Offset
Hs [m]
Offset [m]
DNV-Criteria [m]
Wind Speed [m/s]
[m]
[m/s]
×10^4 sec